Relationships between sounding-based parameters and precipitation field decorrelation

John L. Gensic

National Weather Center Research Experience for Undergraduates, and the University of Saint Francis, Fort Wayne, Indiana[1]

Michael Baldwin*

Cooperative Institute for Mesoscale Meteorological Studies, University of Oklahoma, Norman, Oklahoma

Matthew S. Wandishin*

Cooperative Institute for Mesoscale Meteorological Studies, University of Oklahoma, Norman, Oklahoma

*Also affiliated with the NOAA/OAR National Severe Storms Laboratory, Norman, OK

Research Experience for Undergraduates Final Project
31 July 2004

Corresponding author address: John L. Gensic, 2686 West 25 North, Albion, IN, 46701
Email: gensicjl@studentmail.sf.edu

Abstract:

The understanding of precipitation field evolution is valuable to radar nowcasters and weather modelers. Precipitation field evolution can be evaluated with a decorrelation time that corresponds to how quickly the precipitation field changes from its initial state. Longer decorrelation times are associated with temporally consistent precipitation fields, while short decorrelation times are associated with rapidly changing precipitation fields. The decorrelation times for 246 cases from 1 March 2004 to 6 June 2004 were determined using both Eulerian and Lagrangian perspectives. Lagrangian decorrelation times were nearly 4 times longer than Eulerian times, on the average. No strong linear relationships were determined between the shear and instability parameters collected from nearby observed soundings and the decorrelation time. To further the analysis, Lagrangian decorrelation times were divided into long-lived (decorrelation time > 5 h) and short-lived (decorrelation time < 5) cases. This being done, specific short cases with high CAPE and low helicity could be separated from the long cases. Long cases typically had lower CAPE and higher helicity values, but there were as many short cases meeting these criteria, making discrimination between long-lived and short-lived events difficult in those cases.

1. Introduction

How long is it going to continue raining? Predicting precipitation accurately is an arduous task for two primary reasons. First, it is impossible to know exactly the state of the atmosphere at a given time. Second, the equations describing atmospheric motion are not perfectly known due to the chaotic and nonlinear nature of real fluid systems (Lorenz 1969). Because of the two aforementioned facts, precipitation fields are difficult to properly extrapolate into the future. For proper extrapolation of precipitation fields, advection, growth, and decay of the precipitation field must be determined.

The relationships between environmental parameters and the evolution of precipitation fields are not clearly understood. However, it is not unprecedented to investigate how shear and instability parameters are associated with atmospheric phenomenon. Parameters such as convective available potential energy (CAPE), helicity (H_r), shear, and water vapor content have been shown to impact the discrimination between tornadic and nontornadic low level mesocyclones (Brooks et al. 1994). In addition, derecho and nonderecho systems are somewhat distinguishable by examining proximity soundings for shear and instability parameters, when divided into synoptically strongly- or weakly-forced categories (Evans and Doswell 2001). More closely associated with this project, Zawadzki and Ro (1978) found a relationship between higher surface-based CAPE (SBCAPE) values and maximum precipitation rates. Also Zawadzki et al. (1981) discovered that both mean and maximum rain rates are correlated with thermodynamic parameters. It has yet to be determined clearly to what extent shear and instability parameters can be used to classify precipitation events into long, continuous episodes and shorter-lived, rapidly changing systems.

The question remains whether spatio-temporal coherence of precipitating systems is related to instability and shear parameters. The purpose of this paper is to determine which shear and instability parameters are most closely associated with the movement and development of precipitation fields, by analyzing how sounding-based parameters are related to precipitation field decorrelation time.

2. Literature Review

Previous work that examined precipitation decorrelation time did not reveal strong relationships between decorrelation time and synoptic or mesoscale parameters. That being noted and evaluated further in this work, some studies have suggested that specific mesoscale parameters should stabilize a precipitation event and therefore increase its decorrelation time. For example, Lilly (1986) suggested that high levels of H_r should result in long-lived, coherent convective precipitation events, but this has not been analyzed in relation to a large data set of precipitation decorrelation times. Zawadzki et al. (1994), in an "exploratory study," made an attempt to relate specific parameters with decorrelation times. While this study was the first of its type relating decorrelation times with specific environmental parameters, it only studied 11 warm season precipitation events and did not use a large composite of radar data. In Zawadzki et al. (1994), parameters such as vertical distribution of thermal advection, wind shear energy, and geostrophic vorticity showed no clear relationship with decorrelation time. However, some relationships were noted. A linear relationship between decorrelation time and CAPE was found, with an R^2 value of 0.37 (at the 5% significance level). A linear relationship between decorrelation time and the ratio of CAPE to H_r was also determined, with an R^2 value of 0.85, but this data set was limited to 5 events where the CAPE values were above 850 J kg^{-1}. Finally, a multilinear regression revealed a

relationship between H_r and $\ln(CAPE)$, and decorrelation time, with an R^2 of 0.44 (at 5%-10% significance level). These relationships will be investigated further in the present study by examining more cases and using national composite radar.

Beyond mesoscale and synoptic parameters, Germann and Zawadzki (2002) investigated how Eulerian and Lagrangian perspectives change the decorrelation times for precipitation systems. In that study, Eulerian lifetime determination involved no forecasting of precipitation fields, but involved simply correlating the initial field with the observed field at some later time. The Lagrangian decorrelation time determined was not how quickly the system decorrelated from its fixed initial state, but how quickly the system decorrelated from a Lagrangian forecast, that is, the initial field advected by a predicted wind field. The decorrelation values for the 2002 study were determined by

$$c(\tau) = \frac{\overline{I_o I_f}}{\sqrt{\overline{I_o^2 I_f^2}}} = \frac{\frac{1}{n}\sum_{k=1}^{n} I_o(k) I_f(k)}{\left[\left(\frac{1}{n}\sum_{k=1}^{n} I_o^2(k)\right)\left(\frac{1}{n}\sum_{k=1}^{n} I_f^2(k)\right)\right]^{1/2}}, \tag{1}$$

where $\overline{I_o}$ is the mean of the precipitation field coverage at the initial time, and $\overline{I_f}$ is the mean of the precipitation at the forecast time. The decorrelation time, or lifetime (L), is defined as:

$$L = \int_0^\infty c(\tau) d\tau \tag{2}$$

When $c(\tau)$ follows an exponential law, as in this case, L is the time when the correlation drops below $1/e$, or about 0.37.

Germann and Zawadzki (2002) found Lagrangian decorrelation times to be nearly twice as long as Eulerian decorrelation times. However, that study only examined four cases that were large in coverage area, using a square of radar analysis 2720 km x 2720

5

km. Germann and Zawadzki (2002) noted how decorrelation times decrease at smaller scales of radar resolution as the result of small scale disturbances in motion. Because Lagrangian decorrelation took twice as long as Eulerian, the study revealed that advection explains a significant part of the variation in the precipitation rate at a given location. Germann and Zawadzki (2002) also found that predictability increases as the scale of interest increases, and the smaller, thunderstorm scale is filtered out. While the current study examined the thunderstorm scale, it was in the hope of using proximity sounding data to characterize near storm environments and to see how decorrelation times relate to this smaller scale. The aim of this project was to investigate a range of scales, not leave smaller scales unexamined.

3. Data and Method

a. Data Description

Precipitation events between 1 March 2004 and 6 June 2004 were chosen from University Corporation for Atmospheric Research's (UCAR) case selection database (http://locust.mmm.ucar.edu/case-selection). This website contained national composite radar data in roughly l h intervals, except in specific cases where gaps in the composite data existed. Significant precipitation patterns near United States sounding locations east of the Rocky Mountains close to 00 UTC were noted. Both the initial time a storm was present near a sounding (approximately 328 km (200 mi) from the sounding) and the time the storm seemed to dissipate or move more than 328 km (200 mi) from the sounding location were recorded for the dataset. Domain size was chosen to be small enough that the near storm environment could be adequately measured by the sounding, but large enough that decorrelation and dissipation of the storm could be sufficiently monitored.

6

This size was also used because it is roughly equivalent to the average spacing between sounding locations. The soundings were thus considered representative of the environment in which the storm evolved. Completeness of sounding parameters was required to include a case in this study. If a case's available parameters were incomplete, the case was not used in this study.

Once the locations and beginning times were determined, Stage IV radar data (Fulton et al. 1998) with rainfall hourly accumulations based solely on reflectivity were used for the correlation calculations. Stage IV data is available in hourly intervals at 4 km resolution. A limitation of this data set is correlation values can be computed only at hourly increments. If shorter observation intervals were possible, this would increase the accuracy of decorrelation time calculations.

Sounding-based shear and instability parameters were collected for each event. Each sounding was visually examined for signs of convective contamination. Such soundings represent the storm (or post-storm) environment and not the environment the evolving precipitating system encounters as it progresses and evolves. Cases with contaminated soundings were therefore eliminated from the data set. This reduced the data set from 246 to 147 cases.

The instability measures collected were SBCAPE ($J kg^{-1}$), mixed-layer CAPE (MLCAPE; $J kg^{-1}$), most unstable CAPE (MUCAPE; $J kg^{-1}$), 850-500 mb lapse rate (°C km^{-1}), and 700-500 mb lapse rate (°C km^{-1}). The shear parameters collected were 0-1 km H_r (m^2s^2), 0-3 km H_r (m^2s^2), and 0-6 km shear (m s^{-1}). Along with these parameters, the amount of precipitable water (PW; mm) and the maximum average precipitation were determined for each case.

b. Decorrelation Time

The correlation used in this study is how closely two precipitation fields resemble each other based on:

$$c(\tau) = \frac{\overline{I_i I_\tau}}{\sqrt{\overline{I_i^2}\,\overline{I_\tau^2}}} \qquad (3)$$

Where I_i is the initial precipitation field, I_τ is the precipitation field at time τ, and $c(\tau)$ is the correlation value at a specified time, τ. Notice that the mean is not subtracted from the precipitation fields, as zero precipitation is the "only meaningful reference value" when evaluating precipitation systems, because the average would be always nonzero and very small (Turner et al. 2004). The correlation values are used to determine a decorrelation time or lifetime for each event. This decorrelation time was defined as the time, τ, at which the correlation value drops below 0.5, as used in Zawadzki et al. (1994). Linear interpolation was used to estimate decorrelation times between hourly data available (Figs. 1 and 2).

The grids for precipitation field analysis that were correlated with one another were 644 km (400 mi) by 644 km (400mi) squares, with the sounding location as the center point of the initial grid for precipitation analysis.

Eulerian Lifetime Determination

The lifetimes of precipitation fields meeting the established criteria (nonconvective and complete sounding-based parameters) using an Eulerian persistence model were determined. Using equation (3) as the method for determining correlation between fields at hourly intervals, decorrelation time was estimated (Fig. 1). The Eulerian method of lifetime determination used the sounding location as the center point

8

for every precipitation field correlation calculation. No advection scheme was used to change the center point with time.

Lagrangian Lifetime Determination

The lifetimes of precipitation fields meeting the established criteria were also determined using a Lagrangian advection scheme. The goal of the advection scheme was to follow the initial precipitation field as it advected through the composite of radar coverage. Unlike Germann and Zawadzki (2002), no attempt was made to forecast precipitation fields by shifting the initial field in a particular direction based on an extrapolation of the wind field. The method of translating used here is less sophisticated than their extrapolation.

For each hour beyond the initial time, the precipitation field to be correlated with the initial precipitation field grid was determined by shifting the grid by at most 100 km. Every hour, the grid was shifted to a new center point in which the lowest root mean square error between the new precipitation field and initial field was obtained. The center point shifts were examined to guard against egregious shifts, i.e., reverting back to new precipitation entering the domain. Once a new center point for that next hour was found, the correlation was calculated using equation (3). If this value was below 0.5, then correlation values were no longer determined. If this value remained above 0.5, the process continued to the next hour, where a new center point was determined as the location with the lowest root mean square. By this method, only observed precipitation fields were correlated with other observed precipitation fields. This method differs slightly from the other work involving precipitation decorrelation (i.e. Zawadzki et al.

1994, Germann and Zawadzki 2002, Turner et al. 2004), because in this case, no wind field extrapolation was done.

c. Regression Analysis

Linear Regression

Simple linear regression experiments using decorrelation time as the dependent variable and various sounding-based parameters as the independent variables were performed. This analysis was done for both Eulerian lifetimes and Lagrangian lifetimes. In addition, cases where SBCAPE=0 J kg^{-1} and MLCAPE=0 J kg^{-1} were eliminated, and the sets were analyzed once again. These regressions created a least squares fit line with a correlation value, R^2, which measured the strength of the relationship between each parameter and the decorrelation times.

Logistic Regression

Because linear regression results showed weak relationships between lifetimes and parameters (Table 1), logistic regression (Wilks 1995) was used to attempt to discriminate between long-lived and short-lived events. Logistic regression requires a binary predictand, usually a yes/no outcome. For this reason, the Lagrangian lifetimes were categorized as long (lifetime > 5 h) or short (lifetime < 5 h). This 5 h limit was used because it indicates events that were at least 1 h longer than average. Furthermore, note in the distribution of Lagrangian lifetimes shown in Fig. 4 the density of points above the 5 h threshold is substantially lower than density of points below that mark. Logistic regression fits the variables of linear regression to a nonlinear equation (which produces an S-shaped curve):

$$\hat{y} = \frac{1}{1 + \exp[b_0 + b_1 x_1]} \tag{4}$$

Using this method the dependent variable values are now probabilities that will never exceed one, but should change as the independent variable changes, if there is any predictive skill in the independent variable. In this case, a higher probability should mean a greater likelihood of a long-lived event.

d. Linear Discriminant Analysis

Another technique for classifying or discriminating different types of events, linear discriminant analysis (LDA), was used. Pairs of parameters are arranged into data matrices, one containing the two parameters for long-lived precipitation events, and another containing the same two parameters for short-lived precipitation events. The end result of LDA is a line in the two-parameter space that attempts to separate the long-lived events from the short-lived events based on the means and variances of their respective parameter sets (Appendix A and Wilks 1995).

The LDAs with relatively high Peirce Skill Scores (PSS; Peirce 1884) were then examined more fully, as described below. The PSS is the difference between the probability of detection (POD) and the probability of false detection (POFD) (Richardson 2000). POD is the ratio of the number of events classified correctly by LDA as "long" to the number of observed long events. POFD is the ratio of the number of events classified as "long" but observed as "short" to the number of observed "short" events (Doswell et al. 1990).

Using the discriminating line in the two-dimensional parameter space, a relative operating characteristic (ROC) curve was created (Mason 1982). By shifting the y-intercept of the LDA formally created line, new PODs and POFDs may be determined (See Section 4.d). The set of (POFD, POD) pairs (each associated with a different y-

intercept) can then be used to form a ROC curve. First, the area under each ROC curve was determined with the points from all the y-intercept changes. After this method produced curves that were not smooth, the points that caused concavity were eliminated and the area under the curve was recomputed, giving the area beneath the ROC convex hull (Provost and Fawcett 2001). All areas were calculated using the trapezoidal rule.

4. Results

a. Decorrelation Time

Figures 1 and 2 show the correlation functions for a few sample cases using the Eulerian and Lagrangian approaches, respectively. The average Lagrangian decorrelation time was near 4 h, while Eulerian decorrelation times averaged just greater than 1 h. The correlation values decreased nearly linearly with time, validating the use of linear interpolation for estimating decorrelation time (Figs. 1, 2). Many Eulerian decorrelation times were below 1 h. Because the radar mosaics were only in hourly increments, these Eulerian decorrelation time interpolations may not be good estimates of true decorrelation from the initial state. Still, this 4 to 1 ratio between average Lagrangian and Eulerian lifetimes differs substantially from the Germann and Zawadzki (2002) results that Lagrangian estimates were roughly twice as long as Eulerian lifetimes.

b. Linear Regression

The linear regression analysis experiments revealed no strong correlations between the sounding-based parameters recorded and the Eulerian or Lagrangian decorrelation times. However, certain parameters were more correlated than others, with Eulerian lifetimes having greater correlations to some parameters than did Lagrangian

lifetimes (Table 1). Even the highest correlation values were quite weak, with 0-1 km H_r showing the strongest correlation with Lagrangian lifetime, R^2=0.12 (Fig. 3).

c. Logistic Regression

Because Eulerian lifetimes were closely grouped and many had lifetimes slightly less than one hour, they were not analyzed using logistic regression. The Lagrangian lifetimes were divided into short and long data sets for logistic regression as described in Section 3c and Wilks (1995). This had very little discriminating power to separate long events from short events, but was able to group a selection of cases that were always short. When the ratio of MUCAPE (J kg^{-1}) to 0-1 km H_r (m^{2}s^2) is greater than about 50, the observed precipitation events had decorrelation times less than 5 h (Fig. 5). Also, when the ratio of MUCAPE (J kg^{-1}) to 0-3 km H_r (m^{2}s^2) was greater than 25, all of the observed cases had Lagrangian lifetimes less than 5 h (Fig. 6). For smaller MUCAPE to H_r ratios, systems could be either short-lived or long-lived. The data seems to indicate that long-lived, stable events do not occur in low H_r environments. This is consistent with Lilly's (1986) conclusion that high internal helicity helps to organize storms, leading to more coherent, longer-lived systems.

d. Linear Discriminant Analysis

Relatively high Peirce skill scores determined which linear discriminant analysis parameter sets were selected for further analysis to make ROC curves (Table 2). Adjustments to the y-intercept were made in order to create 20 POD and POFD scores for each linear discriminant analysis scatter plot. In the context of Fig. 7, the POD is the number of triangles appearing above the discrimination line (i.e., correctly classified long-lived systems) to the total number of triangles (i.e., total number of long-lived

systems). Similarly, the POFD is the ratio of the number of circles above the line (i.e., short-lived events incorrectly classified as long-lived) to the total number of circles (i.e., the total number of short-lived events). Notice the high ratio of circles to triangles below the discriminant line compared to the more nearly equal numbers of each above the line. This shows, once again, the ability to isolate some short-lived events, but the long-lived events cannot be distinguished. The (POFD, POD) points associated with each of the 20 y-intercepts were used to create a ROC curve for each pair of parameters (Fig. 8). For each ROC curve an original area was determined by simply adding the trapezoidal areas under the curve.

Each point on the ROC curve represents a possible decision point, but only points lying along the ROC convex hull represent potentially optimal decision points (Provost and Fawcett 2001). That is, there is no user for whom decisions based on the classifier represented by point A in Fig. 8 would provide greater benefit than decisions based on a classifier represented by one of the points on the convex hull. Therefore, the area under the ROC convex hull is a more accurate measure of the usefulness of the classifying system (Figs. 9 and 10, Table 3). The area under the ROC curves indicated some skill in these classifications with ROC areas generally near 0.70, with MUCAPE and 0-1 km H_r as the best pair of discriminators when only cases with positive CAPE values were analyzed.

5. Conclusion

The most significant result of this study was that there were specific short-lived cases that could be distinguished from other cases based on their CAPE and H_r values. While there was no way to determine if an event would be long-lived, the cases where

there was high CAPE and low H_r indicated precipitation fields that decorrelated relatively rapidly. Therefore, these results seem to support the idea that high helicity does favor long-lived systems, as indicated by Lilly (1986).

Direct linear relationships between sounding-based parameters and decorrelation time were not revealed. This could be for many reasons. Possibly, the parameters having the most impact on precipitation evolution were not included in the analysis. Also, the sounding-based parameters may not have been truly representative of the environment in which the precipitation evolved. If this was the case, model sounding data, such as from the RUC model, could be used in the future to increase the likelihood that the information is more representative of the near storm environment (e.g. Thompson et al. 2003).

The unique Lagrangian advection that was used in this study makes it difficult to compare these findings to previous work (e.g. Germann and Zawadzki 2002, Zawadzki et al. 1994, Turner et al. 2004). Therefore, direct comparisons with the marginal relationships found in Zawadzki et al. (1994) would not be appropriate. However, whereas Zawadzki et al. (1994) found some strong linear correlations between decorrelation times and some environmental parameters, all linear correlations in this study were very weak. Also, it may be significant that the Lagrangian decorrelation times determined in the current study were about four times as long as the Eulerian times. This is different from Germann and Zawadzki's (2002) determination of Lagrangian lifetimes as being twice as long as Eulerian lifetimes.

15

the REU program. Finally, the help of Dr. Harold Brooks with the linear discriminant

analysis was greatly appreciated.

Appendix A (Wilks 1995):

Data matrices $[X_L]$ and $[X_S]$ represent two-parameter arrays for long and short cases, respectively. The mean of the data matrix throughout the array is denoted:

$$\bar{x}_g = \left[\frac{1}{n_g} \sum_{i=1}^{n_g} x_{i,1}, \frac{1}{n_g} \sum_{i=1}^{n_g} x_{i,2} \right] \qquad g = l, s \tag{5}$$

Where 1 and 2 represent the two parameters and n_g is the number of long or short cases in the array. The covariance matrices ($[S_L]$ and $[S_S]$) are calculated using the $[X_L]$ and $[X_S]$ data arrays. The pooled estimate of the dispersion of these data arrays is found by:

$$[S_{pooled}] = \frac{(n_L - 1)[S_L] + (n_S - 1)[S_S]}{(n_L + n_S - 2)} \tag{6}$$

The direction (d_1) in the two-parameter space that can best be used to distinguish the long and short events is determined by:

$$d_1 = [S_{pooled}]^{-1}(\bar{x}_l - \bar{x}_s) \tag{7}$$

Now, a new discrimination variable may be found that is the projection of the midpoint between the means of the long and short data set in the two parameter space. This variable is a scalar, δ_1, also known as Fisher's linear discrimination function and is found by:

$$\bar{\delta}_1 = d_1^T \frac{\bar{x}_L + \bar{x}_S}{2} \tag{8}$$

This value can be used to classify previously unseen events. Once an event has its location in the two parameter space transposed onto d_1, then it can be compared to δ_1 and placed into a long-lived or short-lived category appropriately. For example, an event will be assigned to the category (short or long) above the discriminant line if:

$$d_1^T y - \bar{\delta}_1 \geq 0 \qquad (9)$$

However if the event is transposed onto d_1 and:

$$d_1^T y - \bar{\delta}_1 \leq 0 \qquad (10)$$

Then this event would be assigned to the category below the discriminant line.

REFERENCES

Brooks, H. E., C. A. I. Doswell, and J. Cooper, 1994: On the Environments of Tornadic and Nontornadic Mesocyclones. *Wea. Forecasting*, **9,** 606-618.

Doswell, C. A. I., R. Davies-Jones, and D. L. Keller, 1990: On Summary Measures of Skill in Rare Event Forecasting Based on Contingency Tables. *Wea. Forecasting*, **5,** 576-585.

Evans, J. S. and C. A. I. Doswell, 2001: Examination of Derecho Environments Using Proximity Soundings. *Wea. Forecasting*, **16**, 329-342.

Fulton, R.A., J. P. Breidenbach, D.-J. Seo, D. A. Miller, and T. O'Bannon, 1998: The WSR-88D Raingall Algorithm. *Wea. Forecasting*, **13**, 377-395.

Germann, U. and I. Zawadzki, 2002: Scale-Dependence of the Predictability of Precipitation from Continental Radar Images. Part I: Description of the Methodology. *Mon. Wea. Rev.*, **130,** 2859-2873.

Lilly, D. K., 1986: The Structure, Energetics and Propagation of Rotating Convective Storms. Part II: Helicity and Storm Stabilization. *J. .Atmos. Sci.*, **43,** 126-140.

Lorenz, E. N., 1969: Three Approaches to Atmospheric Predictability. *Bull. Amer. Meteor. Soc.*, **50**, 345-349.

Mason, I., 1982: A model for assessment of weather forecasts. *Aust. Meteor. Mag.*, **30,** 291-303.

Peirce, C.S., 1884: The numerical measure of the success of predictions. *Science*, **4**, 453-454.

Provost, F., and R. Fawcett, 2001: Robust classification for imprecise environments. *Machine Learning*, **42**, 203-231.

Richardson, D.S., 2000: Skill and relative economic value of the ECMWF ensemble prediction system. *Q. J. R. Meteor. Soc.*, **126**, 649-667.

Thompson, R. L., R. Edwards, J. A. Hart, K. L. Elmore, and P. Markowski, 2003: Close Proximity Soundings within Supercell Environments Obtained from the Rapid Update Cycle. *Wea. Forecasting*, **18,** 1243-1261.

Turner, B. J., I. Zawadzki, and U. Germann, 2004: Predictability of Precipitation from Continental Radar Images. Part III: Operational Nowcasting Implementation (MAPLE). *J. Appl. Meteor.*, **43,** 231-248.

Wilks, D. S., 1995: *Statistical Methods in the Atmospheric Sciences*. Vol. 59, Academic Press, 467 pp.

Zawadzki, I., and C. U. Ro, 1978: Correlations between Maximum Rate of Precipitation and Mesoscale Parameters. *J. Appl. Meteor.*, **17,** 1327-1334.

____, E. Torlaschi, and R. Sauvageau, 1981: The Relationship between Mesoscale Thermodynamic Variables and Convective Precipitation. *J. Atmos. Sci.*, **38,** 1535-1540.

____, J. Morneau, and R. Laprise, 1994: Predictability of Precipitation Patterns: An Operational Approach. *J. of Appl. Meteor.*, **33,** 1562-1571.

Table 1. Summary of linear regression between decorrelation time and sounding-based

parameters.

Greater than 0.10 Linear Regression Correlation Coefficients

Perspective	Data Set	# of Cases	Parameter	R^2
Eulerian	Greater than zero SBCAPE and MUCAPE	72	max. ave. precip.	0.18
Eulerian	Including zero SBCAPE and MUCAPE	82	0-1 km helicity	0.16
Eulerian	Including zero SBCAPE and MUCAPE	82	0-3 km helicity	0.10
Lagrangian	Greater than zero SBCAPE and MUCAPE	68	0-1 km helicity	0.12

Table 2. Skill Scores for the LDA without any y-intercept alterations. PSS=POD-POFD

(Richardson 2000).

Skill Scores for Original LDA line

Parameters for LDA	PSS (POD-POFD)
With all cases	
MUCAPE, 0-1 km helicity	0.19
MUCAPE, 0-3 km helicity	0.14
SBCAPE, 0-1 helicity	0.20
SBCAPE, 0-3 helicity	0.17
850-500mb LR, 0-3 km helicity	0.29
When CAPE>0	
MUCAPE, 0-1 km helicity	0.27
MUCAPE, 0-3 km helicity	0.29
log SBCAPE, log 0-1 km helicity	0.33
log SBCAPE, log 0-3 km helicity	0.43
log MUCAPE, log 0-1 km helicity	0.34
log MUCAPE, log 0-3 km helicity	0.30
850-500 mb LR, 0-3 km helicity	0.31

Table 3. Trapezoidal areas under the ROC curve. Elimination of cases with 0 CAPE in any of the three CAPE classes, increased the skill of the LDA classification. Using MUCAPE and 0-1 km helicity proves to be the best discriminators.

ROC Area Scores

Parameter Combination	Regular Area	Convex Hull Area
log MUCAPE log 0-1 km helicity, positive CAPE cases	0.70	0.72
MUCAPE log 0-1 km helicity, postive CAPE cases	0.68	0.69
MUCAPE 0-1 km helicity, all CAPE cases	0.64	0.63
MUCAPE 0-1 km helicity, positive CAPE cases	0.71	0.74
SBCAPE 0-1 km helicity, positive CAPE cases	0.70	0.72
SBCAPE 0-1 km helicity, all CAPE cases	0.62	0.66
850-500 LR 0-3 km helicity, positive CAPE cases	0.71	0.74

Eulerian Correlation v. Time
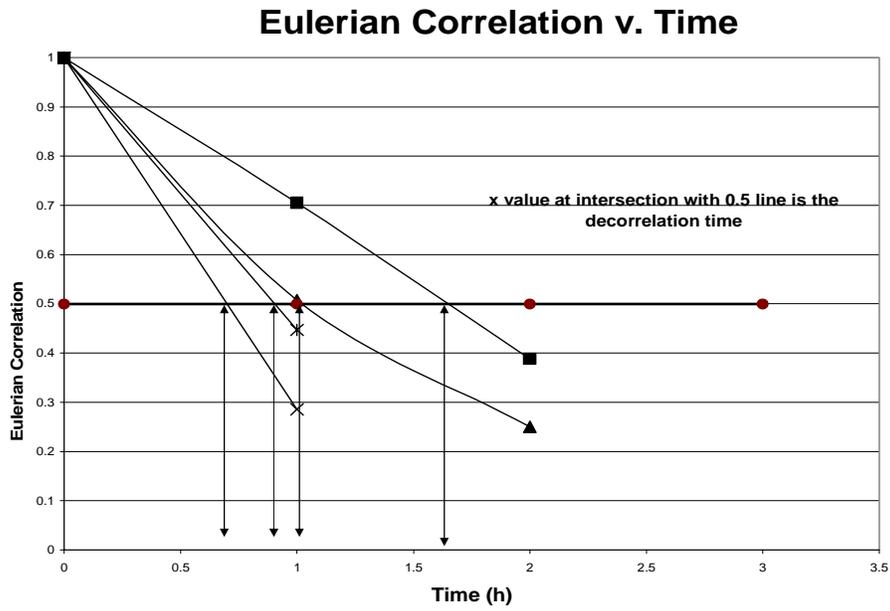
Fig. 1. Sample Eulerian correlation values decreasing with time. Each curve represents a random case selected from among the 147 cases examined.

Lagrangian Correlation v. Time
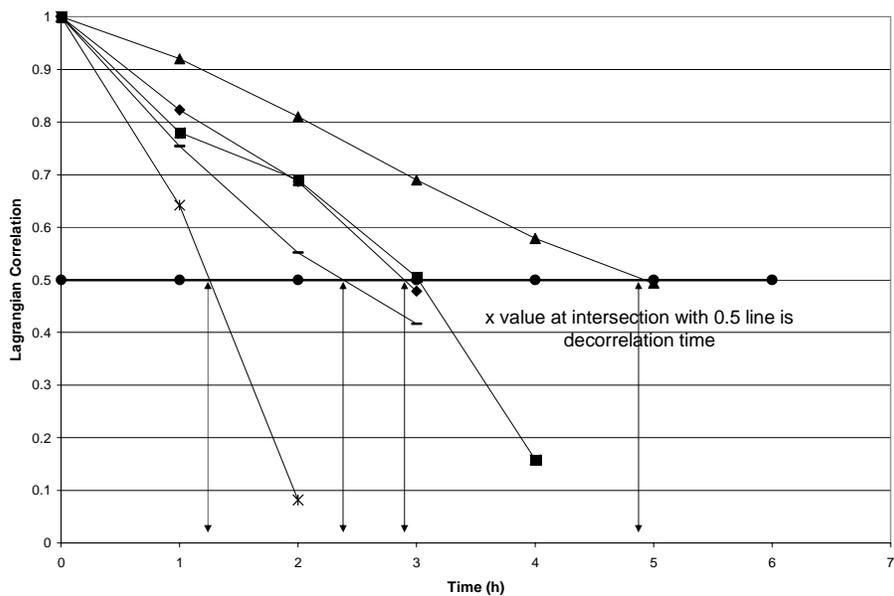
Fig. 2. As in Fig. 1, but for Lagrangian correlations.

Lagrangian Lifetime v. 0-1 km Helicity
(positive CAPE cases)
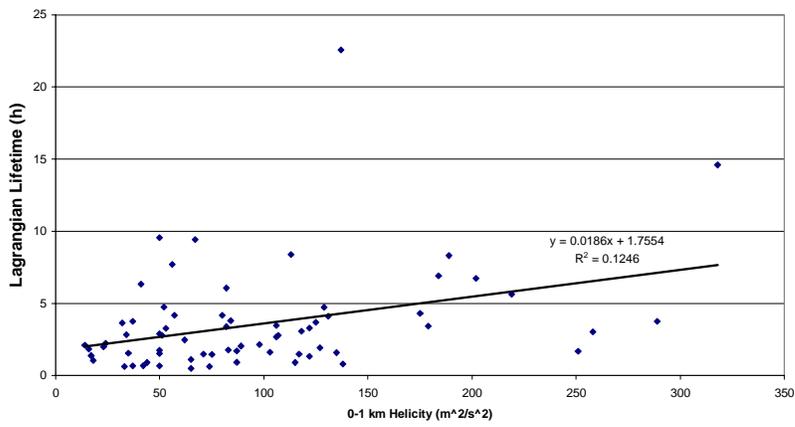
Fig. 3. Least squares fit between 0-1 km helicity and Lagrangian decorrelation time.
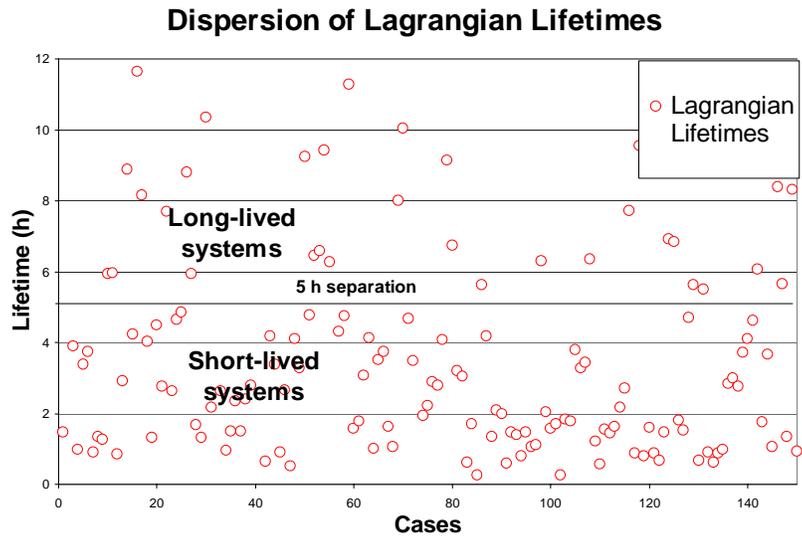
Fig. 4. Categorization of systems as short-lived (lifetime < 5 h) and long-lived (lifetime > 5 h).

Long or Short v. MUCAPE / 0-1 km Helicity
(positive CAPE cases)
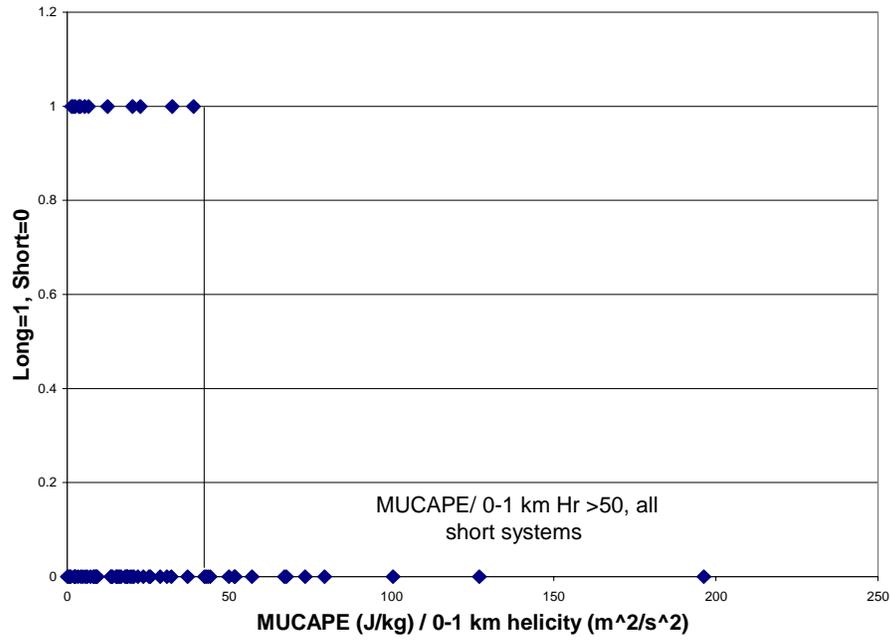
Fig. 5. Separation of long and short Lagrangian lifetimes using ratio of MUCAPE to 0-1 km H_r.

Long or Short v. MUCAPE / 0-3 km Helicity

(positive CAPE cases)

MUCAPE/ 0-3 km helicity > 25, all short systems

Y-axis: Long=1, Short=0

X-axis: MUCAPE (J/kg) / 0-3 km Helicity (m^2/s^2)
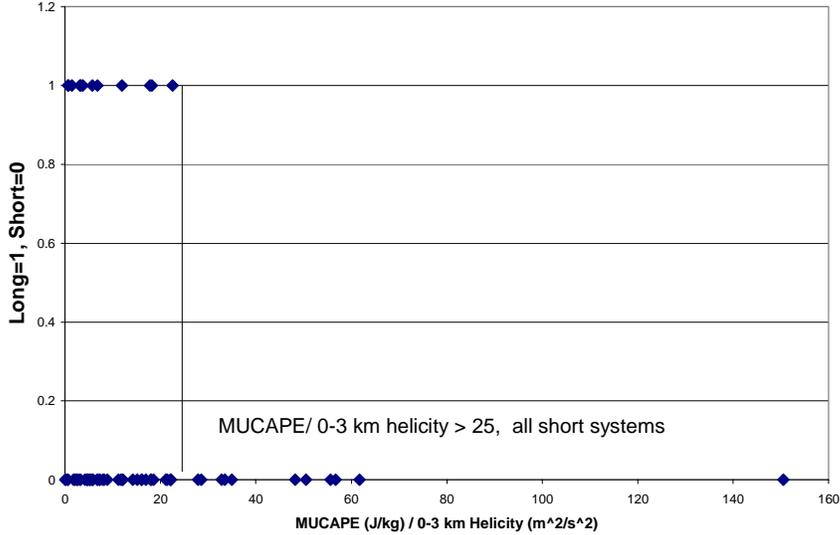
Fig 6. As in Fig. 5, except for the ratio of MUCAPE to 0-3 km H_r.

LDA: MUCAPE and 0-1 km Helicity
(positive CAPE cases)
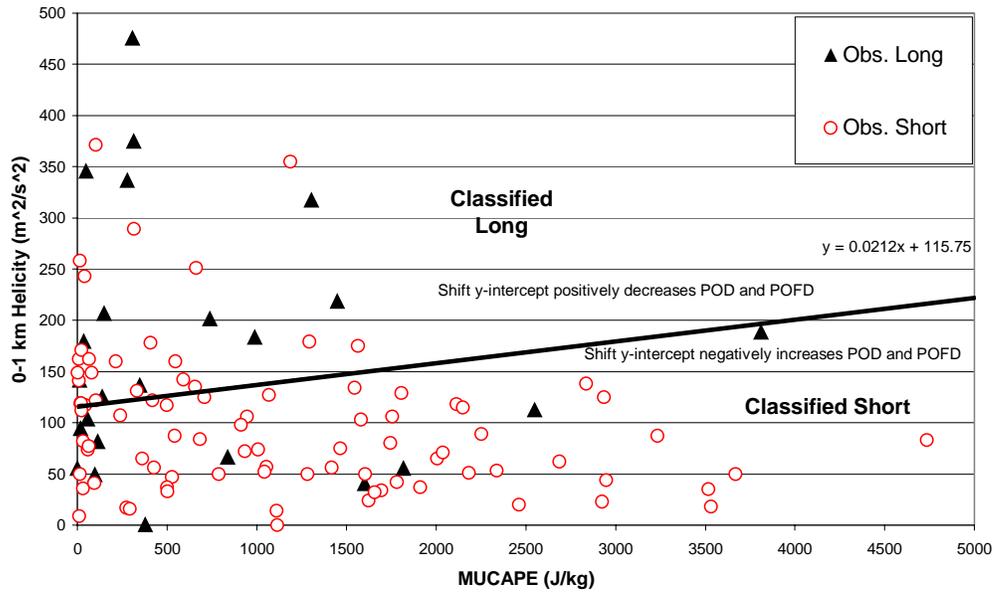
Fig 7. LDA of long and short cases using MUCAPE and 0-1 km helicity. When y-intercepts are shifted, this creates a series of POD and POFD values that can be evaluated on a ROC curve.

POD v. POFD for LDA with MUCAPE and 0-1 km Helicity

(positive CAPE cases)
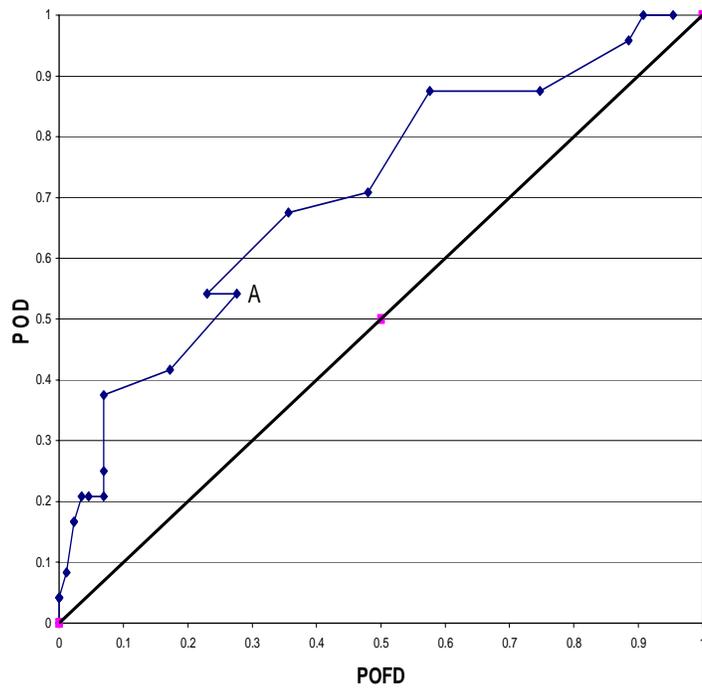
Fig. 8. ROC curve without concavity eliminated for LDA using MUCAPE and 0-1 km helicity. The points are created using a series of y-intercept alterations of the LDA created discriminant line (Fig 6).

ROC Convex Hull
POD v. POFD for LDA with MUCAPE and 0-1 km Helicity
(positive CAPE cases)
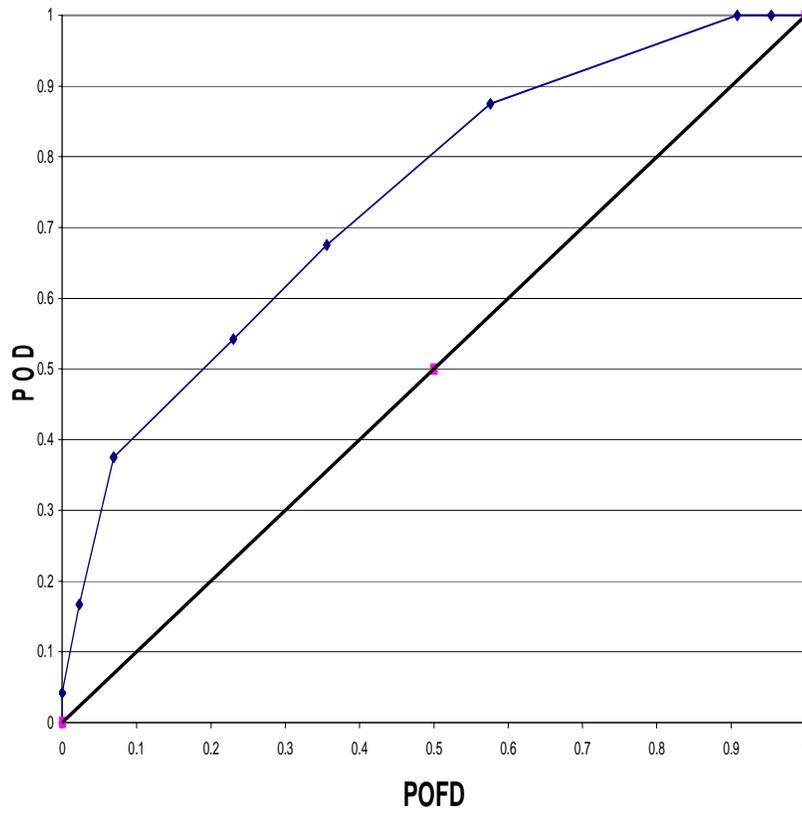
Fig. 9. ROC curve with concave values eliminated for LDA with MUCAPE and 0-1 km

helicity.

ROC Convex Hull
POD v. POFD for LDA with 850-500 mb Lapse Rates
and 0-3 km Helicity
(positive CAPE cases)
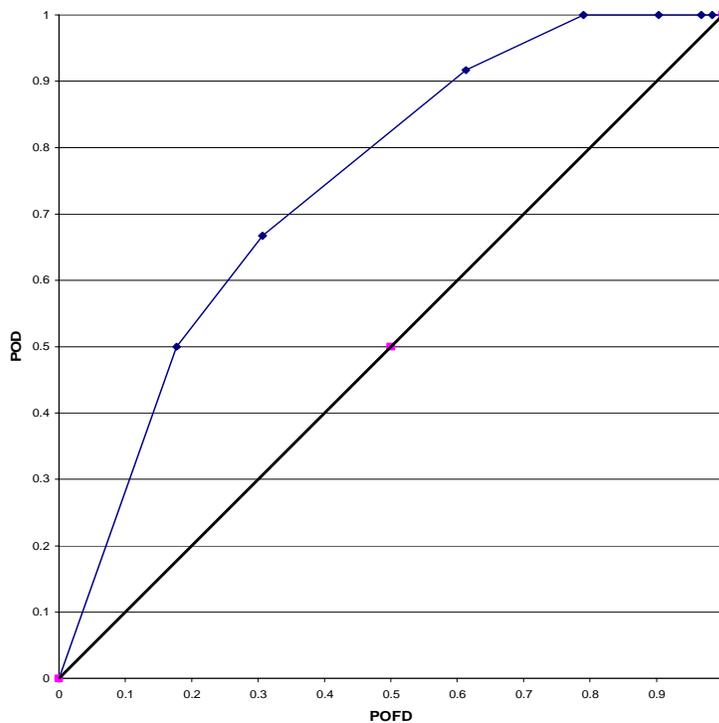
Fig. 10. As in Fig. 9, for LDA using 850-500 mb lapse rate and 0-3 km H$_r$.